Biomedical Microdevices (2020) 22: 43
https://doi.org/10.1007/s10544-020-00498-0

Penetrating glassy carbon neural electrode arrays for brain-machine interfaces

Biao Chen[1,2] · Boshen Zhang[3] · Chaoyang Chen[2,4] · Jie Hu[1] · Jin Qi[1] · Tao He[1] · Pan Tian[1] · Xinuo Zhang[5] · Guoxin Ni[4] · Mark Ming-Cheng Cheng[2,3]

Published online: 6 June 2020

Abstract

This paper presents a fabrication method for glassy carbon neural electrode arrays that combines 3D printing and chemical pyrolysis technology. The carbon electrodes have excellent biological compatibility and can be used in neural signal recording. A pretreated Si wafer is used as the substrate for 3D printing, and then, stereolithography 3D printing technology is employed to print photosensitive resin into a cone shape. Next, chemical pyrolysis is applied to convert the 3D prints into glassy carbon electrodes and modify the electrochemical performance of the carbon electrodes. Finally, the glassy carbon electrodes are packed with conductive wires and PDMS. The proposed fabrication method simplifies the manufacturing process of carbon materials, and electrodes can be fabricated without the need of deep reactive ion etching (DRIE). The height of the carbon electrodes is 1.5 mm, and the exposure area of the tips is 0.78 mm^2, which is convenient for the implantation procedure. The specific capacitance of the glassy carbon arrays is higher than that of a platinum electrode (9.18 mF/cm^2 vs 3.32 mF/cm^2, respectively), and the impedance at 1 kHz is lower (7.1 kΩ vs 8.8 kΩ). The carbon electrodes were tested *in vivo*, and they showed excellent performance in neural signal recording. The signal-to-noise ratio of the carbon electrodes is 50.73 ± 6.11, which is higher than that of the Pt electrode (20.15 ± 5.32) under the same testing conditions. The proposed fabrication method of glassy carbon electrodes provides a novel approach to manufacture penetrating electrodes for nerve interfaces in biomedical engineering and microelectromechanical systems.

Keywords Carbon electrode · Implantable electrode · Penetrating neural recording · 3D printing

Biao Chen and Boshen Zhang contributed equally to this work.

Electronic supplementary material The online version of this article (https://doi.org/10.1007/s10544-020-00498-0) contains supplementary material, which is available to authorized users.

✉ Chaoyang Chen
cchen@wayne.edu

✉ Jie Hu
hujie@sjtu.edu.cn

[1] State Key Laboratory of Mechanical System and Vibration, Shanghai Jiao Tong University, Shanghai, China

[2] Department of Biomedical Engineering, Wayne State University, Detroit, MI, USA

[3] Electrical and Computer Engineering, Wayne State University, Detroit, MI, USA

[4] Department of Rehabilitation Medicine, First Affiliated Hospital of Fujian Medical University, Fuzhou, China

[5] Department of Orthopedics, China Capital Medical University affiliate Beijing Chaoyang Hospital, Beijing, China

1 Introduction

Multifunctional neural implants play an essential role in the brain-machine interface (BMI) and functional electrical stimulation (Musk 2019). A major goal for neural implantation is to integrate the implants into the nervous system without severely damaging tissue (Stieglitz et al. 2000). However, most of the neural interfaces are manufactured into planar geometries, which means that they have a limited ability to be implanted into the nervous system or to record signals in 3D neural tissues.

Metals (platinum and tungsten) and silicon materials are widely used for neural stimulation and recording (Johnson et al. 2013; Schander et al. 2015; Scholvin et al. 2015) due to their excellent mechanical and electronic properties (Cogan 2008). However, metals and silicon materials have limited capability in detecting molecular events during stimulation because of slow electron transfer and limited detection windows. Moreover, rigid materials such as Pt and silicon are not suitable for use in long-term implant procedures because of

the mechanical mismatch between tissues and rigid materials, which can easily damage human tissues or cause infection.

Carbon materials are promising materials for preparing neural electrodes because of their excellent biocompatibility, including carbon black (Alcántara et al. 2001; Liu et al. 2012), carbon nanotubes (Bilgi and Ayranci 2016; David-Pur et al. 2014; Gupta et al. 2018; Lin et al. 2009; Yi et al. 2015), graphene (Kuzum et al. 2014; Yan et al. 2012), glassy carbon (Afkhami et al. 2016; Asadian et al. 2017; Mani et al. 2016), etc. Some researchers have also tried to manually assemble carbon fiber electrode arrays as implant electrodes to record a single unit signal (Patel et al. 2015, 2016). Glassy carbon has also been verified to be a promising electrode material for neural interfaces due to its good electrical properties, electrochemical stability, and chemical inertness (Hirabayashi et al. 2015; Vomero et al. 2017; Wang et al. 2010). Carbon electrodes using pyrolysis photoresist (Brooksby and Downard 2004; Ranganathan et al. 2000) and SU-8 (Wang et al. 2005) have been demonstrated, but they typically have limited stiffness to penetrate the cortex.

In the traditional carbon material manufacturing process, it is difficult to fabricate millimeter-high carbon electrodes due to the slow reaction speed or costly clean-room equipment. Therefore, we proposed a new fabrication method of combining 3D printing and chemical modification to manufacture millimeter-high glassy carbon electrodes.

3D printing is a promising additive manufacturing (AM) technique for fabricating objects with complex geometries or delicate internal structures (Chia and Wu 2015; Wang et al. 2016). According to the difference in working principles, the most commonly used 3D printing techniques can be divided into five main categories: selective laser sintering (SLS), fused deposition modeling (FDM), inkjet printing (IP), stereolithography (SLA), and direct ink writing (DIW). Among the five categories, SLA is widely used in the fields of biomedical engineering and tissue engineering (Arcaute et al. 2010) because of its high flexibility and excellent printing resolution.

For the first time, this paper presents a novel method of manufacturing millimeter-high, implantable glassy carbon electrodes to probe sophisticated electrical and chemical environments in a brain. By combining SLA 3D printing, chemical pyrolysis, and direct transfer with parylene, multiple carbon electrodes have been integrated without the need of deep reactive ion etching (DRIE). This work adapts stereolithography to create high-aspect-ratio polymer microstructures. With optimal pyrolysis treatments, the microstructures have been converted to carbon electrodes with excellent electrochemical and chemical properties. An array of carbon neural electrodes has been preliminarily tested *in vivo*, where the release of neural signals provides useful information for closed-loop control in neural stimulation.

Our objective is to integrate high-density, mechanically robust glassy carbon using low-cost 3D printing and chemical modification to simultaneously perform neural stimulation/recording and chemical sensing. The carbon electrode can be fabricated in any arbitrary 3D geometry, which has been found to be challenging with conventional silicon micromachining. The height of our implantable carbon electrodes is 1.5 mm, with a tip exposure area of 0.78 mm^2. We optimized the parameters for the 3D printer to obtain the desired structure directly printed on a Si substrate. The processing parameters for pyrolysis were changed to make the structure more conductive and less deformable. Then, we used parylene coating to directly transfer the structure from the Si substrate. The electrochemical performance of the carbon electrodes was evaluated by electrochemical impedance spectroscopy (EIS) and cyclic voltammetry (CV). An electrophysiological experiment was conducted to measure the neural signals *in vivo* using carbon electrodes with electrical stimulation at the sciatic nerve.

2 Method

2.1 Thermogravimetric analysis (TGA)/derivative thermogravimetry (DTG)

The most critical point of pyrolysis processing is temperature control during polymer carbonization. Different polymers have different chemical bonds and structures that require different processing parameters for pyrolysis, including the maximum heating temperature, heating environment, heating rate, and cooling method. Frequently, the temperature control of the polymer can be optimized based on the thermogravimetric analysis (TGA) and derivative thermogravimetry (DTG) results. The pyrolysis conditions of negative photoresist (SU-8) have previously been studied by analyzing the TGA results. To prepare the samples, two 2 cm × 2 cm films were directly printed by using a 3D printer, and one 2 cm × 2 cm SU-8 film was made by using the photolithography method as a reference sample. Before the TGA/DTG testing, one of the 3D-printed samples was preheated in an oven at 250 °C for two days.

2.2 Device fabrication

The fabrication process of carbon neural electrode arrays is shown in Fig. 1. A Si wafer was used as the substrate for 3D printing. Because the material characteristics of the Si wafer and the photosensitive resin had significant differences, the adhesion between the Si wafer and the 3D prints was quite weak. As shown in Fig. 1a, an SU-8 layer was deposited on a Si wafer, and then, the SU-8 layer was patterned into a micropillar array (80 μm height, 20 μm diameter) by

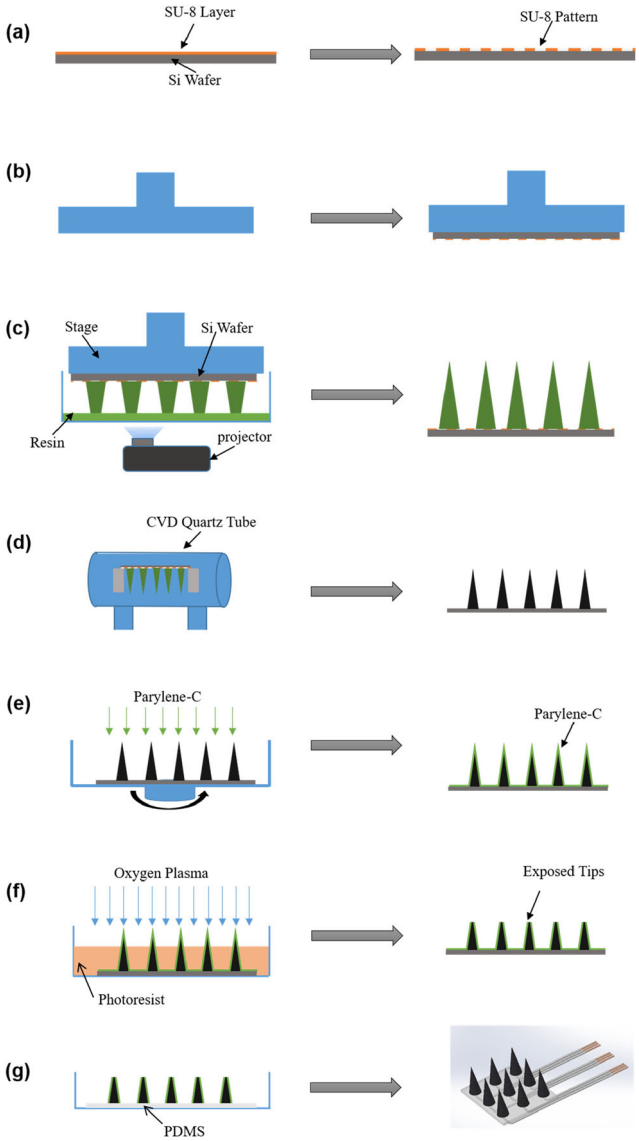

Fig. 1 Fabrication process of high-density carbon neural electrode arrays **a** SU-8 patterning on the Si wafer **b** gluing the Si wafer on the stage **c** 3D printing **d** pyrolysis **e** parylene-C coating **f** oxygen plasma **g** packing

lithography. The SU-8 layer was used as a buffer layer between the Si wafer and the 3D prints to make the 3D prints tightly contact the substrate. The size of the 3D-printed cone array was 4.5 mm in height and 0.9 mm in diameter, so the micropillar array would have a subtle influence on the 3D prints in the pyrolysis process.

Before 3D printing, the Si wafer was glued on the stage by a hot glue gun. The 3D printing process was conducted with a Titan 2 3D printer (Kudo 3D, Dublin, CA), and the working principle of Titan 2 was based on SLA. The photosensitive resin was 3DSR General Black, which consisted of 5% photoinitiator, 29% acrylate monomer and 66% acrylate oligomer (the percentage was calculated by weight). As shown in Fig. 1c, the stage with the Si wafer was positioned at the bottom of the resin container and moved up gradually during printing. After finishing 3D printing, we used acetone to soften the glue so that we could remove the Si wafer from the printing stage. Then, the printed object was washed with isopropyl alcohol (IPA) to remove residual resin on its surfaces. Next, the object was placed in a UV chamber for an additional 15 mins of postcuring to fully cure the object.

The pyrolysis process is shown in Fig. 1d. Before pyrolysis, the print was pretreated in an oven at 250 °C for 48 h. Then, the 3D-printed cone array was placed in a CVD quartz tube with a three-step temperature control pyrolysis process. The temperature was first increased from room temperature to 350 °*C* with a 10 °*C*/min heating rate. The temperature was then held at 350 °*C* for one hour. Next, the temperature was increased from 350 °*C* to 550 °*C* with a 2 °*C*/min heating rate, which provided enough time for gas evolution, followed by holding at 550 °*C* for one hour. Then, the temperature was increased to 900 °*C* with a 5 °*C*/min heating rate and held at 900 °*C* for another hour. Finally, the carbon electrodes were naturally cooled to room temperature. A low flow-rate (300 sccm) inert gas (90% argon/10% hydrogen) environment was used in the pyrolysis process to allow the gases to be released gradually.

After pyrolyzing, a five micron parylene-C film was coated on the surface of the electrode array by the spin-coating method, as shown in Fig. 1e. The purpose of the parylene-C film coating was to electrically insulate the device and facilitate direct transfer of the carbon array from the Si substrate. As shown in Fig. 1f, oxygen plasma was used to expose the tips of the carbon electrode arrays. The exposed tips of the device were electrically conductive. Next, the carbon array was transferred from the Si wafer, and conductive wires were manually linked to the bottom of the carbon arrays with conductive silver epoxy. Finally, the device was placed on a PDMS substrate; the final device is shown in Fig. 1g.

2.3 Electrochemical analysis

To verify the performance of the carbon electrode arrays, electrochemical impedance spectroscopy (EIS) and cyclic voltammetry (CV) measurements were taken with a Gamry potentiostat controlled by Gamry Framework software. Moreover, we used commercial Pt microelectrodes as the comparison electrodes. For all measurements, a Faraday cage was used to block electromagnetic field noise, and the probes were submerged in 1x phosphate-buffered saline (PBS, pH 7.4) solution. The electrochemical analysis was performed on a three-electrode system. A Ag/AgCl electrode was used as the reference electrode, a Pt electrode was chosen as the counter electrode, and a carbon electrode served as the working electrode. EIS measurements were obtained by applying a 10 mV alternating current with frequencies ranging from 1 Hz to 100 kHz. CV measurements were obtained in a

potential window ranging from −0.7 V to 1.2 V, at scan rates from 20 mVs^{-1} to 200 mVs^{-1}, scanning for 6 cycles.

2.4 Electrophysiological experiment

The carbon electrodes were tested *in vivo* to record neural signals from the brains of rats. The Animal Investigation Committee at Wayne State University approved all the procedures. Adult male Sprague-Dawley rats weighing 550–600 g ($n = 6$) were used for the electrophysiological experiment. Rats were first anesthetized by using 5% isoflurane to render them unconscious and then using an intraperitoneal injection of butorphanol (0.1 mg kg^{-1}), ketamine hydrochloride (43 mg kg^{-1}), and xylazine (7 mg kg^{-1}). Supplemental doses were used as needed to maintain anesthesia during the experiment.

The surgical procedures include cutting the dura to expose the right somatosensory cortex and exposing the left sciatic nerve. As shown in Fig. 2, carbon electrodes were placed on the right somatosensory cortex to record the neural signals, and a pair of Teflon-coated Pt wires with a 2 mm bare tip were placed on a wax shell to hook the sciatic nerve. Stimulus pulses (1 Hz, 2 ms duration) were applied to the Pt wires to stimulate the sciatic nerve to evoke neural signals with amplitudes ranging from 0.1 to 3 V. The neural signal and stimulus voltage were simultaneously recorded (sampling rate at 1 kHz) using a BIOPAC data acquisition system MP-36 (BIOPAC Inc., Goleta, CA). The sampling rate of the data acquisition system was 1 kHz, with an amplification gain of 1000x. The neural signal recording channel was filtered from 5 Hz to 35 Hz.

3 Results and discussion

3.1 Thermal analysis

The TGA/DTG data of SU-8 and the 3D-printed polymer are shown in Fig. 3. It is evident that significant weight loss for SU-8 starts at approximately 350°*C* and continues until 1100 °*C*, and the total mass loss is 90.84% (see Fig. 3a). However, in the result of the 3D-printed polymer, the weight loss steps start earlier and include three different regions. The first mass loss step occurred soon after heating until approximately 200°*C*, totaling 2.2%. The next stage, with 20.81% mass loss, occurred from approximately 200 °*C* to 350°*C*, while the final loss of 68.09% occurred at 350 °*C* and continued until 550°*C*; beyond that point, there was not much weight loss until the temperature reached 1100 °*C* (see Fig. 3b and c). This result was also confirmed by the DTG data (shown in Fig. 3), which showed a similar trend. The DTG curve of the 3D-printed polymer showed different reaction peaks at 148 °C, 305 °C, and 422 °C, and there were no additional sharp peaks in the curve at higher temperatures.

To further understand the reactions taking place and the gases evolving during pyrolysis, gas analysis was performed. A synchronized gas analysis system employing Fourier transform infrared (FTIR) spectroscopy was used to determine the gases evolved during pyrolysis. In the 3D-printed polymer, the FTIR results showed a mass-loss step at approximately 212 °*C*, indicating possible water (H_2O), carbon dioxide (CO_2) and organic volatile evolution. With increasing temperature, the mass-loss steps appeared at approximately 212–315 °*C*, indicating possible 2-ethyl-1-butanol (C_6H_{12}) and carbon dioxide (CO_2) evolution, and mass-loss steps appeared at approximately 315–440 °*C*, indicating possible methyl propyl ketone ($C_5H_{10}O$) and 5-methyl-2-hexanone ($C_7H_{14}O$) evolution.

3.2 Device fabrication

In general, the electrochemical properties and mechanical characteristics of glassy carbon mainly depend on the degree of carbonization (Lee et al. 2008; Singh et al. 2002). The relationship of the temperature vs the degree of carbonization was tested by EDX analysis, and the results are shown in Fig. 4. A higher pyrolysis temperature yielded a higher percentage of carbon components in the electrode. The percentage of carbon increased by 40% when the pyrolysis temperature increased from 300 °C to 900 °C.

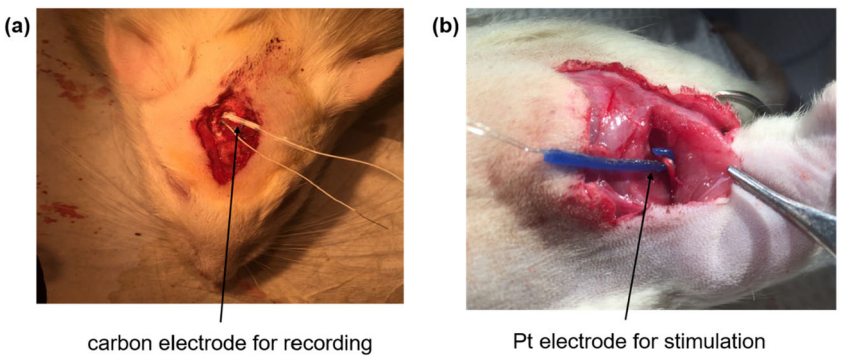

Fig. 2 **a** Carbon electrode placement for neural signal recording **b** Pt electrodes stimulate the sciatic nerve to evoke a neural signal

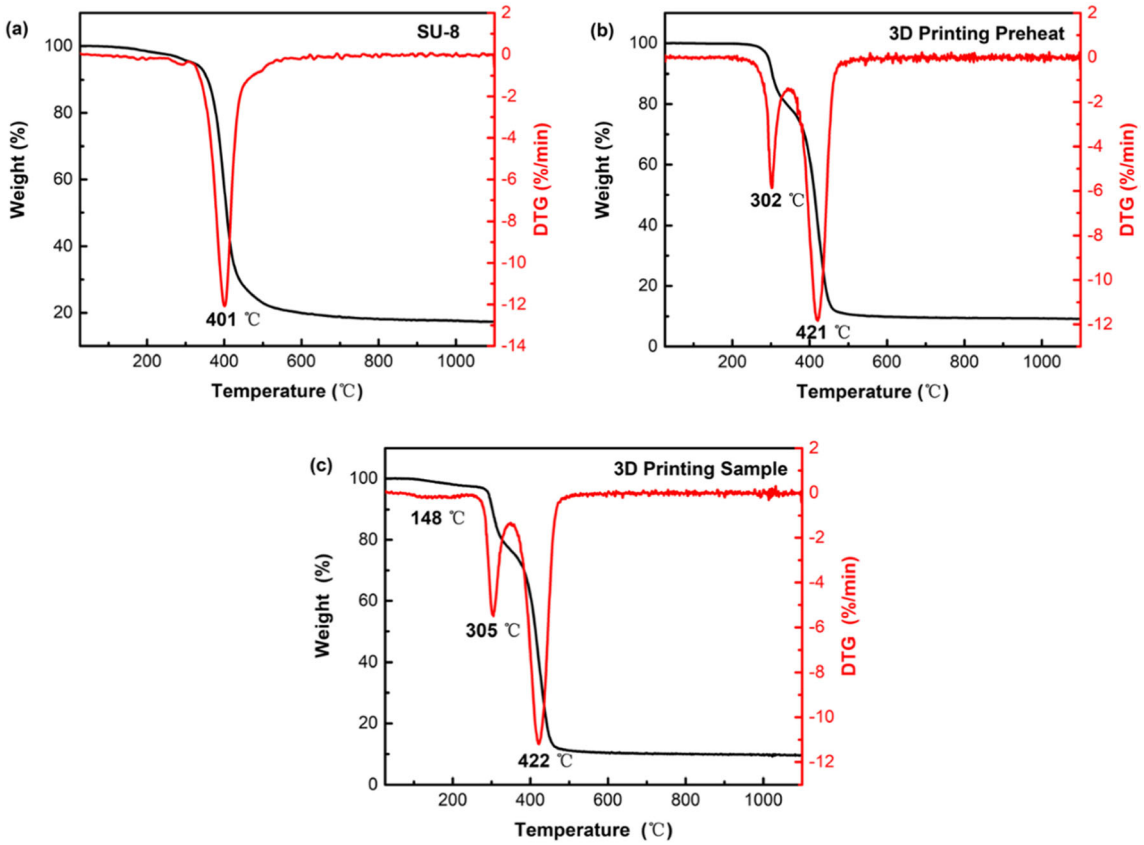

Fig. 3 TGA/DTG results of three different samples

The fabricated carbon electrode arrays are not always adherent to the substrate after pyrolysis. The main reasons include poor adhesion between the substrate and polymer, gas evolution during pyrolysis, and thermal internal stress caused by the difference in the coefficients of thermal expansion of the substrate and polymer. To minimize deformation and create an electrode array with high resolution and structure transfer fidelity, novel techniques were developed in this study using a nontraditional pyrolysis recipe, including adding a high-temperature preheating process, flipping the object during pyrolysis, and enhancing adhesion by adding an SU-8 buffer layer.

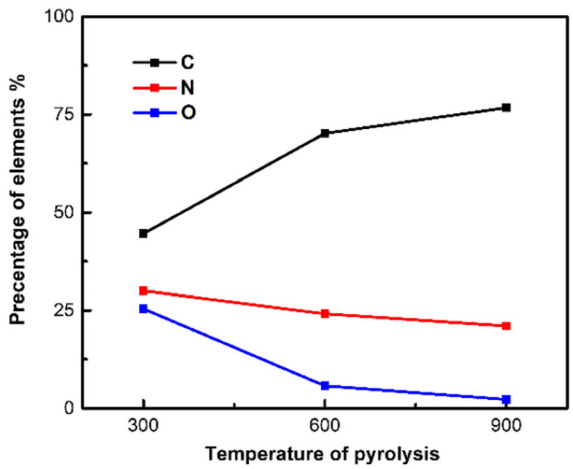

Fig. 4 Element percentage of carbon electrodes vs pyrolysis temperature

Figure 5a and b shows the 3D-printed structure under an optical microscope. The 3D-printed polymer has poor adhesion with the silicon substrate. Before 3D printing, a 20 μm SU-8 layer was coated and patterned as a buffer layer to improve adhesion. After 3D printing, the print was preheated at a high temperature (250 °*C*) under vacuum for 48 h to limit the cone shape deformation during pyrolysis. Shape deformation could occur as the heating temperature increased above the glass transition temperature of the 3D-printed polymer (250 °*C*). At those temperatures, the polymer softened and could cause the cone shape to bend in a random direction. We found that preheating the printed structure at the glass transition temperature before pyrolysis could avoid the polymer softening process.

Adhesion was affected by gas evolution and thermal stress during pyrolysis. In the experiment, three designs were used to reduce adhesion issues. First, the print was flipped and placed in the furnace to reduce the stress and help the gas escape. The reason was that during pyrolysis, most of the stress is concentrated at the carbon/substrate interface, and the shrunken structure makes carbon accumulate at the interface, blocking gas escape. Flipping the printed structure could avoid stress

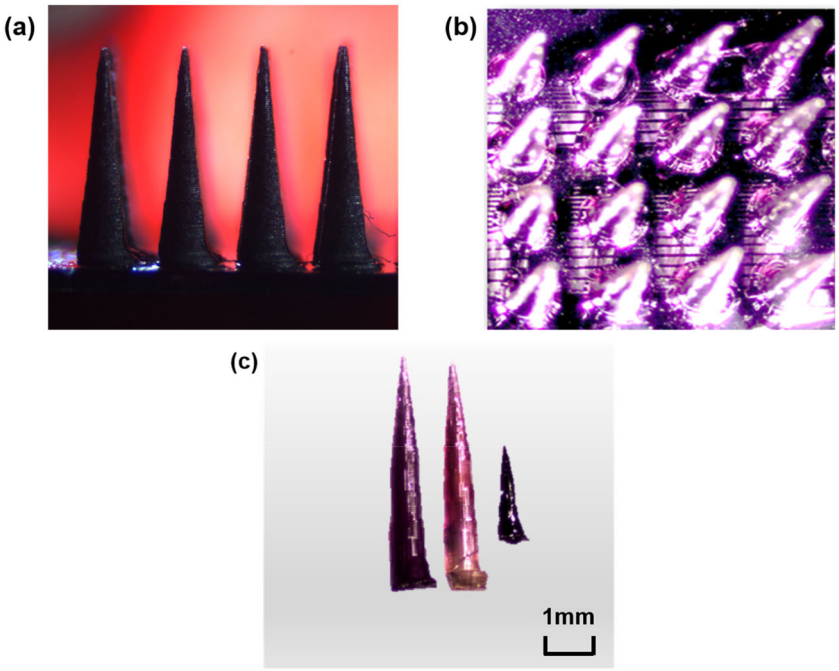

Fig. 5 **a** 3D-printed structure on a silicon wafer **b** 3D-printed structure after preheating **c** Comparison of the structure, preheated structure and structure after pyrolysis

accumulation and limit gas evolution, which was beneficial to the adhesion of the structure during pyrolysis. A three-step heating process was then used to control the heating temperature by monitoring the temperature during each step using TGA.

As shown in Fig. 5c, there was an obvious decrease in volume after pyrolysis. In the longitudinal direction, the structure shrank by 59.6%, and in the width direction, the structure shrank by 36.3%. Because the structure was a cone, the shrinkage in volume was 83.6%.

Figure 6a shows a 4 × 4 glassy carbon array on a flexible PDMS substrate, Fig. 6b presents an SEM view of a 2 × 2 glassy carbon array with a magnification factor of 50x, and the inset image shows the tip of the glassy carbon with a magnification factor of 966x. After calibration under a microscope, the diameter of the exposed tip is 20 μm, and the height of the glassy carbon tip is 1.5 mm.

3.3 Electrochemical characterization

The electrochemical behavior of carbon arrays and commercial Pt microelectrodes were studied utilizing cyclic voltammetry (CV) and electrochemical impedance spectroscopy (EIS). CV was used to quantify the charge storage capacity (CSC), and EIS was used to observe the charge transport dynamics. Figure 7a shows the CV curves of the carbon electrodes at a voltage window from −0.7 V to 1.2 V and scan rates ranging from 20 mV/s to 200 mV/s. Figure 7b shows the CV curves of the carbon electrodes and Pt electrodes at a scan rate of 100 mV/s. The specific capacitance of the electrodes was

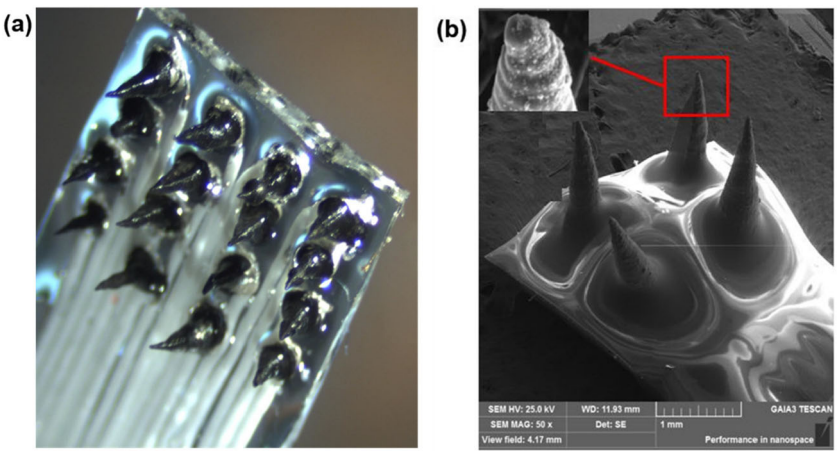

Fig. 6 **a** an encapsulated 4 × 4 glassy carbon array in optical microscope **b** a SEM view of 2 × 2 glassy carbon array (50x), the insertion is partial amplified view of glassy carbon tip (966x)

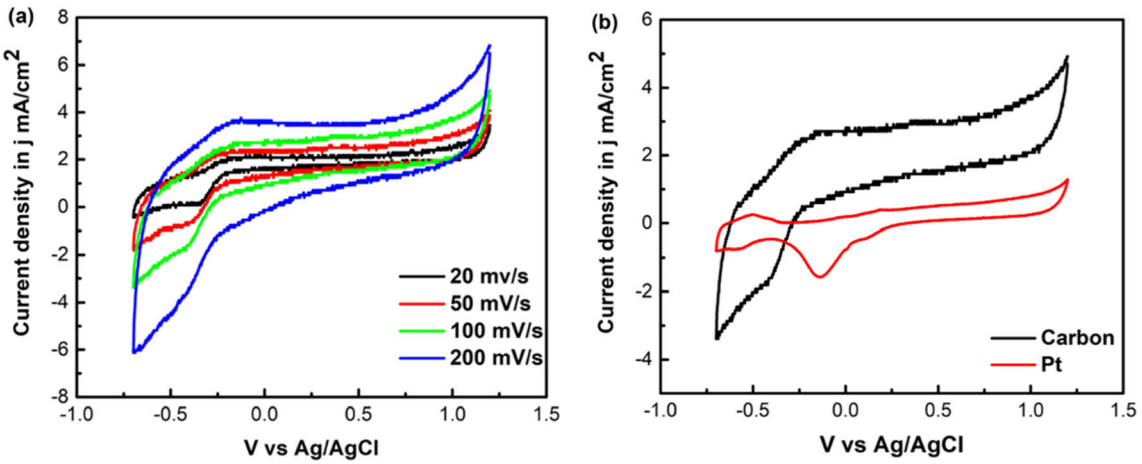

Fig. 7 **a** Cyclic voltammetry curves of carbon electrodes at scan rates from 20 mV/s to 200 mV/s **b** Cyclic voltammetry plot of carbon and Pt electrodes vs Ag/AgCl in 1x PBS solution at scan rate of 100 mV/s

calculated by MATLAB (Mathworks, Natick, MA) scripts using the following formula:

$$C = \frac{\int_{E_1}^{E_2} i(E)d(\mathrm{E})}{[2A(E_2 - E_1)v]}$$

where E1 is the lower limit of the potential, E2 is the upper limit of the potential, i(E) is the current, d(E) is the differential of the potential, A is the exposure area of the electrodes, and v is the scan rate.

The exposure area A of the carbon electrode was 0.78 mm^2, and for the Pt electrode, the value was 0.61 mm^2. The results showed that the carbon electrode had a higher specific capacitance than the Pt electrode (9.18 mF/cm^2 vs 3.32 mF/cm^2, respectively). The CV curves showed that the peak current magnitude was correlated with the electrode area, diffusion coefficient, redox species, concentration and voltage scan rate. The results showed that the carbon electrode had better electrochemical properties than the commercial Pt electrode (see Fig. 7b).

EIS has been used as an additional approach to evaluate the electrochemical behavior of carbon arrays and commercial Pt microelectrodes. The EIS measurement can determine the changes in charge transfer resistance with the different voltages applied. These resistance data can be used to obtain information about the electrochemical reaction rate. For quantitative comparisons of the charge transfer resistance, Fig. 8a summarizes EIS plots of the carbon and Pt electrodes, which were fitted using the equivalent circuit models, and provides further insight into the electrical properties of the electrodes. As shown in Fig. 8a, the impedance values of the carbon electrodes were lower than those of the Pt electrode in the frequency band from 10 Hz to 30 kHz. The impedance values at 1 kHz usually represent the efficiency of a recording electrode because 1 kHz is the physiologically relevant spiking frequency of neurons. For the carbon electrode, the impedance at 1 kHz is 7.1 kΩ, and for the Pt electrode, the value is 8.8 kΩ, which is 23.9% higher than that of the carbon electrode.

The Nyquist plots for carbon electrodes and the equivalent circuit models are reported in Fig. 8b. The graphs plot the imaginary impedance (Zimage) against the real impedance (Zreal) at each testing frequency. The solution resistance can be obtained by reading the real axis value at the high-frequency intercept, which corresponds to the charge transfer at the electrode interface. The real axis (X-axis) value at the low-frequency region is the sum of the polarization resistance. The solution resistance resulted from the diffusion transfer process. In this model, the composition of the equivalent circuit includes the electrolyte resistance (Rs), charge transfer resistance (Rct) in parallel with a constant phase element (CPE) and Warburg diffusion impedance (W). The constant phase element is defined as an unideal capacitor, which can be expressed as $Z_{CPE} = \frac{1}{(j\omega)^{\alpha} Y_0}$, where Y_0 represents the capacitance and α is a constant related to the different behavior compared to that of a pure capacitors ($Y_0 = 1$ for a pure capacitor). The EIS parameters of carbon in the equivalent circuit and in the equivalent circuit RS represent the resistance of the PBS solution. The model shows a good fitting result for both carbon and Pt electrodes. The EIS parameters for carbon electrodes obtained through fitting the experimental data to the model are $R_S = 2916\ \Omega$, $R_{CT} = 1522\ \Omega$, Z_{CPE} with $Y_0 = 7.42\ e^{-7}\ S*s^{\alpha}$ and $\alpha = 0.65$, and $Z_W = 2.6\ e^{-7}\ S*s^{1/2}$.

3.4 Neural signal recording

Neurophysiological experiments were performed *in vivo* to evaluate the performance of the carbon electrode in recording neural signals. The detailed animal preparation procedures and signal recording method are described in section 2.4. The left sciatic nerve was exposed to place a pair of Pt wire hooked electrodes for electrical stimulation. For neural

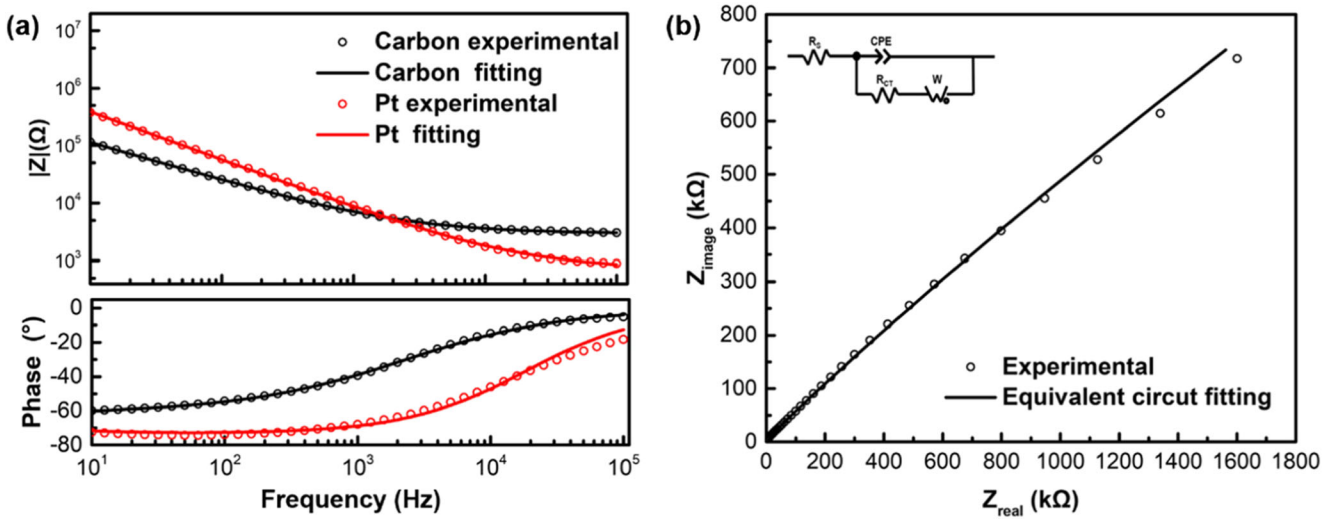

Fig. 8 **a** Bode plot of the magnitude and phase of impedance vs frequency **b** Experimental data and fitting result of the carbon electrode

recording, the rat cerebral cortex was exposed by a medical drill, and the recording electrodes were placed on the surface of the right somatosensory cortex. This placement is because the right somatosensory cortex receives the somatosenory afferent nerve signals from the left limbs.

Figure 9a and b shows neural signal recorded by carbon and Pt electrode at stimulation voltage of 0.1 V and 0.8 V. At low stimulation voltage (0.1 V), the carbon electrode clearly recorded the neural signals evoked by electrical stimulation, while the neural signals recorded by the Pt electrode were drowned out by noise (Fig. 9a). At a higher stimulation voltage (0.8 V), the Pt electrode and carbon electrode showed similar peak values of evoked potential, but the carbon electrode had a more stable resting potential (Fig. 9b). After stimulation, the carbon electrode returned to the resting potential quicker than the Pt electrode.

Because we used a periodic stimulation *in vivo* experiment, valid signals were defined as the signal that we collected when stimulation was applied, while noise signals were defined as the signal that we collected when the stimulation was not applied. The signal-to-noise ratio (SNR) can be calculated by the following equation:

$$SNR = 10*\log_{10}\left(\frac{Singal\ Power}{Noise\ Power}\right) = 10*\log_{10}\left(\frac{\frac{\int_{t_1}^{t_2} x_0^1(t)dt}{t_2-t_1} - \frac{\int_{t_0}^{t_1} x_0^2(t)dt}{t_1-t_0}}{\frac{\int_{t_0}^{t_1} x_0^2(t)dt}{t_1-t_0}}\right),$$

where $x_1(t)$ represents the amplitude of the valid signals, and $x_0(t)$ represents the amplitude of noise. t_0 is the time that we start collecting signals, t_1 is the time when stimulation is applied, and t_2 is the time when stimulation is stopped.

The SNR of the neural signals recorded in the cerebral cortex of six adult rats (at a stimulation voltage of 0.8 V) are listed in Table 1. The average SNR of the carbon electrodes was 50.73 ± 6.11, while that of the Pt electrodes was 20.15 ± 5.32. The results showed that carbon electrodes had higher SNRs (*t* test, $p < 0.001$).

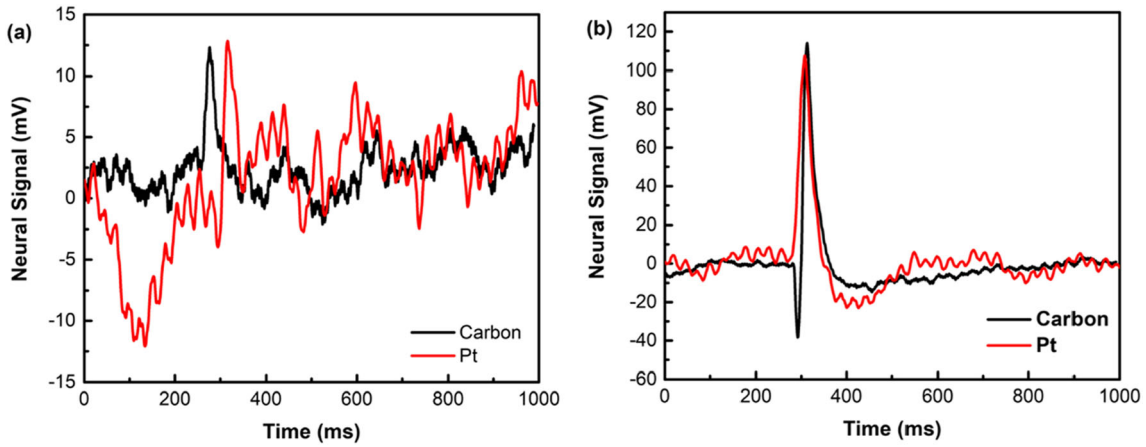

Fig. 9 *In vivo* neural signal recording of rats using carbon and Pt electrodes **a** EEG signals recorded by carbon and Pt electrodes at a stimulation voltage of 0.1 V. **b** EEG signals recorded by carbon and Pt electrodes at a stimulation voltage of 0.8 V

Table 1 The SNR of neural signals for six adult rats

	1	2	3	4	5	6
Carbon	49.53	42.68	55.74	57.92	44.82	53.71
Pt	19.81	12.37	23.45	25.46	15.32	24.47

4 Conclusion

In this paper, we demonstrated a novel method using 3D printing technology to fabricate millimeter-high glassy carbon neural implant arrays. Compared with the traditional MEMS and semiconductor fabrication process, pyrolysis of a variety of geometries of 3D-printed objects, without shapes or height limitations, represents a new carbon electrode fabrication technique, which has potential applications in the fabrication of 3D carbon-based electrodes for sensors. Although a very high percentage of shrinkage occurred during pyrolysis in terms of both height and width, the optimized three-step pyrolysis process maintained the 3D structure of the original 3D geometric design. Penetrating, low-cost glassy carbon electrode arrays were successfully fabricated. The electrodes can be used as both recording and stimulating electrodes for electrical as well as electrochemical signals. In the experiment, the specific capacitance of the carbon electrode was 9.18 mF/cm^2, and the electrode also had low impedance (7.1 kΩ) at 1 kHz, which was beneficial for recording bioelectrical signals in the brain. The electrophysiological experiment showed that the glassy carbon arrays have a higher SNR than that of commercialized Pt electrodes while recording neural signals *in vivo*. This work represents an innovative approach toward realizing advanced penetrating neural probes for better resolution neural recording.

Acknowledgments The experiment was performed at Wayne State University. The carbon electrodes were fabricated in the Nano Fabrication Core (nFab) Laboratory at Wayne State University. *In vivo* animal electrode testing and neurophysiological studies were performed in the Robotic Rehabilitation Laboratory, Department of Biomedical Engineering, at Wayne State University. This research is supported by the Special Program for Innovation Method of the Ministry of Science and Technology, China (2018IM020100), National Natural Science Foundation of China (51975360, 51775332, 51675329), National Social Science Foundation of China (17ZDA020), and the Cross Fund for Medical and Engineering of Shanghai Jiao Tong University (IH2018QNB03, YG2017QN61).

Availability of data and material Thermogravimetric analysis, electrochemical experiment, neurophysiological experiments data is available.
Code availability Not applicable.

Funding information Special Program for Innovation Method of the Ministry of Science and Technology, China (2018IM020100), National Natural Science Foundation of China (51975360, 51775332, 51675329), National Social Science Foundation of China (17ZDA020), and the Cross Fund for Medical and Engineering of Shanghai Jiao Tong University (IH2018QNB03, YG2017QN61).

Compliance with ethical standards

Conflicts of interest/competing interests Not applicable.

References

A. Afkhami, A. Bahiraei, T. Madrakian, Gold nanoparticle/multi-walled carbon nanotube modified glassy carbon electrode as a sensitive voltammetric sensor for the determination of diclofenac sodium. Mater. Sci. Eng. C **59**, 168–176 (2016)

R. Alcántara, J.M. Jiménez-Mateos, P. Lavela, J.L. Tirado, Carbon black: A promising electrode material for sodium-ion batteries. Electrochem. Commun. **3**, 639–642 (2001)

K. Arcaute, B. Mann, R. Wicker, Stereolithography of spatially controlled multi-material bioactive poly (ethylene glycol) scaffolds. Acta Biomater. **6**, 1047–1054 (2010)

E. Asadian, S. Shahrokhian, A.I. Zad, F. Ghorbani-Bidkorbeh, Glassy carbon electrode modified with 3D graphene–carbon nanotube network for sensitive electrochemical determination of methotrexate. Sens. Actuator B-Chem. **239**, 617–627 (2017)

M. Bilgi, E. Ayranci, Biosensor application of screen-printed carbon electrodes modified with nanomaterials and a conducting polymer: Ethanol biosensors based on alcohol dehydrogenase. Sens. Actuator B-Chem. **237**, 849–855 (2016)

P.A. Brooksby, A.J. Downard, Electrochemical and atomic force microscopy study of carbon surface modification via diazonium reduction in aqueous and acetonitrile solutions. Langmuir **20**, 5038–5045 (2004)

H.N. Chia, B.M. Wu, Recent advances in 3D printing of biomaterials. J. Biol. Eng. **9**, 4 (2015)

S.F. Cogan, Neural stimulation and recording electrodes. Annu. Rev. Biomed. Eng. **10**, 275–309 (2008)

M. David-Pur, L. Bareket-Keren, G. Beit-Yaakov, D. Raz-Prag, Y. Hanein, All-carbon-nanotube flexible multi-electrode array for neuronal recording and stimulation. Biomed. Microdevices **16**, 43–53 (2014)

S. Gupta, C. Murthy, C.R. Prabha, Recent advances in carbon nanotube based electrochemical biosensors. Int. J. Biol. Macromol. **108**, 687–703 (2018)

M. Hirabayashi, B. Mehta, B. Nguyen, S. Kassegne, DNA immobilization on high aspect ratio glassy carbon (GC-MEMS) microelectrodes for bionanoelectronics applications. Microsyst. Technol. **21**, 2359–2365 (2015)

L. Johnson, J. Wander, D. Sarma, D. Su, E. Fetz, J. Ojemann, Direct electrical stimulation of the somatosensory cortex in humans using electrocorticography electrodes: A qualitative and quantitative report. J. Neural Eng. **10**, 036021 (2013)

D. Kuzum et al., Transparent and flexible low noise graphene electrodes for simultaneous electrophysiology and neuroimaging. Nat. Commun. **5**, 5259 (2014)

J.A. Lee, S. Hwang, J. Kwak, S.I. Park, S.S. Lee, K.-C. Lee, An electrochemical impedance biosensor with aptamer-modified pyrolyzed carbon electrode for label-free protein detection. Sens. Actuator B-Chem. **129**, 372–379 (2008)

C.-M. Lin, Y.-T. Lee, S.-R. Yeh, W. Fang, Flexible carbon nanotubes electrode for neural recording. Biosens. Bioelectron. **24**, 2791–2797 (2009)

G. Liu et al., A mesoscopic platinized graphite/carbon black counter electrode for a highly efficient monolithic dye-sensitized solar cell. Electrochim. Acta **69**, 334–339 (2012)

V. Mani, M. Govindasamy, S.-M. Chen, R. Karthik, S.-T. Huang, Determination of dopamine using a glassy carbon electrode modified with a graphene and carbon nanotube hybrid decorated with

molybdenum disulfide flowers. Microchim. Acta **183**, 2267–2275 (2016)

E. Musk, An integrated brain-machine interface platform with thousands of channels. J. Med. Internet Res. **21**, e16194 (2019)

P.R. Patel, K. Na, H. Zhang, T.D. Kozai, N.A. Kotov, E. Yoon, C.A. Chestek, Insertion of linear 8.4 μm diameter 16 channel carbon fiber electrode arrays for single unit recordings. J. Neural Eng. **12**, 046009 (2015)

P.R. Patel et al., Chronic in vivo stability assessment of carbon fiber microelectrode arrays. J. Neural Eng. **13**, 066002 (2016)

S. Ranganathan, R. Mccreery, S.M. Majji, M. Madou, Photoresist-derived carbon for microelectromechanical systems and electrochemical applications. J. Electrochem. Soc. **147**, 277–282 (2000)

A. Schander, E. Tolstosheeva, V. Biefeld, L. Kempen, H. Stemmann, A. Kreiter, W. Lang, in *2015 Transducers-2015 18th International Conference on Solid-State Sensors, Actuators and Microsystems (TRANSDUCERS)*. Design and fabrication of multi-contact flexible silicon probes for intracortical floating implantation (IEEE, 2015), pp. 1739–1742

J. Scholvin, J.P. Kinney, J.G. Bernstein, C. Moore-Kochlacs, N. Kopell, C.G. Fonstad, E.S. Boyden, Close-packed silicon microelectrodes for scalable spatially oversampled neural recording. IEEE Trans. Biomed. Eng. **63**, 120–130 (2015)

A. Singh, J. Jayaram, M. Madou, S. Akbar, Pyrolysis of negative photoresists to fabricate carbon structures for microelectromechanical systems and electrochemical applications. J. Electrochem. Soc. **149**, E78–E83 (2002)

T. Stieglitz, M. Schuettler, J.-U. Meyer, Micromachined, polyimide-based devices for flexible neural interfaces. Biomed. Microdevices **2**, 283–294 (2000)

M. Vomero et al., Highly stable glassy carbon interfaces for long-term neural stimulation and low-noise recording of brain activity. Sci. Rep. **7**, 40332 (2017)

C. Wang, G. Jia, L.H. Taherabadi, M.J. Madou, A novel method for the fabrication of high-aspect ratio C-MEMS structures. J. Microelectromech. Syst. **14**, 348–358 (2005)

Y. Wang, L. Pham, G.P.S. de Vasconcellos, M. Madou, Fabrication and characterization of micro PEM fuel cells using pyrolyzed carbon current collector plates. J. Power Sources **195**, 4796–4803 (2010)

J. Wang, A. Goyanes, S. Gaisford, A.W. Basit, Stereolithographic (SLA) 3D printing of oral modified-release dosage forms. Int. J. Pharm. **503**, 207–212 (2016)

J. Yan et al., Advanced asymmetric supercapacitors based on Ni (OH) 2/graphene and porous graphene electrodes with high energy density. Adv. Funct. Mater. **22**, 2632–2641 (2012)

W. Yi et al., A flexible and implantable microelectrode arrays using high-temperature grown vertical carbon nanotubes and a biocompatible polymer substrate. Nanotechnology **26**, 125301 (2015)